ISSN 1674-1056
http://cpb.iphy.ac.cn
http://iopscience.iop.org/cpb
中国物理 B
Chinese Physics
中国物理
Chinese Physics B

Homogeneous transparent device and its layered realization

Cheng-Fu Yang(杨成福), Ming Huang(黄铭), Jing-Jing Yang(杨晶晶), Fu-Chun Mao(毛福春), Ting-Hua Li(李廷华), Peng Li(黎鹏), Peng-Shan Ren(任鹏姗)

Citation: Chin. Phys. B . 2018, 27(12): 124101. **doi:** 10.1088/1674-1056/27/12/124101
Journal homepage: http://cpb.iphy.ac.cn; http://iopscience.iop.org/cpb

What follows is a list of articles you may be interested in

Computational and experimental verification of a wide-angle metamaterial absorber

Chao Chen(陈超), Wang Jun(王君)
Chin. Phys. B . 2017, 26(4): 044101. **doi:** 10.1088/1674-1056/26/4/044101

Optimization of loss and gain multilayers for reducing the scattering of a perfect conducting cylinder

Zhen-Zhong Yu(余振中), Guo-Shu Zhao(赵国树), Gang Sun(孙罡), Hai-Fei Si(司海飞), Zhong Yang(杨忠)
Chin. Phys. B . 2016, 25(7): 074101. **doi:** 10.1088/1674-1056/25/7/074101

Inverse design-based metamaterial transparent device and its multilayer realization

Li Ting-Hua, Huang Ming, Yang Jing-Jing, Yuan Gang, Cai Guang-Hui
Chin. Phys. B . 2014, 23(5): 054102. **doi:** 10.1088/1674-1056/23/5/054102

Design of two-dimensional elliptically cylindrical invisible cloaks with multiple regions

Luo Xiao-Yang, Liu Dao-Ya, Liu Jin-Jing, Dong Jian-Feng
Chin. Phys. B . 2014, 23(5): 054101. **doi:** 10.1088/1674-1056/23/5/054101

Manipulating surface plasmon waves by transformation optics: Design examples of beam squeezer, bend, and omnidirectional absorber

Yu Zhen-Zhong, Feng Yi-Jun, Wang Zheng-Bin, Zhao Jun-Ming, Jiang Tian
Chin. Phys. B . 2013, 22(3): 034102. **doi:** 10.1088/1674-1056/22/3/034102

Homogeneous transparent device and its layered realization*

Cheng-Fu Yang(杨成福)[1], Ming Huang(黄铭)[1,†], Jing-Jing Yang(杨晶晶)[1,‡], Fu-Chun Mao(毛福春)[1], Ting-Hua Li(李廷华)[2], Peng Li(黎鹏)[1], and Peng-Shan Ren(任鹏姗)[1]

[1] *School of Information Science and Engineering, Wireless Innovation Laboratory of Yunnan University, Kunming* 650091, *China*
[2] *Technology Center of China Tobacco Yunnan Industrial Corporation, Kunming* 650231, *China*

(Received 18 June 2018; revised manuscript received 14 August 2018; published online 10 November 2018)

Arbitrarily shaped electromagnetic transparent devices with homogeneous, non-negative, anisotropic and generic constitutive parameters are proposed based on linear transformation optics, which provides the flexibility for device design that is applicable for the practical fabrication. To remove the anisotropic property, a layered structure is developed based on effective medium theory. Simulation results show that with sufficient layers, the performance of the layered transparent device is nearly as perfect as an ideal device, and it is able to protect an antenna without sacrificing its performance. The feasibility of designing a transparent device by using natural isotropic materials instead of metamaterials would dramatically reduce the difficulty of fabrication and further promote the practicality of the device.

Keywords: transformation optics, transparent device, metamaterials, effective medium theory

PACS: 41.20.Jb, 78.20.Bh, 78.67.Pt **DOI:** 10.1088/1674-1056/27/12/124101

1. Introduction

Transformation optics (TO) achieve arbitrary control of field distribution by changing the equivalent physical parameter distribution of materials in the physical space, providing a powerful instrument for the flexible design of metamaterial devices.[1–3] The most prominent application of the TO method might be the design of cloaks,[4–14] which can hide arbitrary objects from exterior electromagnetic illumination and suppress all the scattered waves. Besides cloaks, several metamaterial-based functional devices have also been investigated in either theory or experiment.[15–29] Among various novel applications, transparent devices have recently attracted widespread attention due to their ability to protect the device inside without affecting their performance, and they have shown great potential in antenna protection. By using the compressing or stretching transformation method, a two-dimensional (2D) transparent device was first proposed by Yu *et al.*[30] Later, the arbitrarily shaped transparent devices with either conformal or non-conformal boundaries were proposed by Yang *et al.*[31] and Mei *et al.*,[32] and the general expressions of material parameters were developed. However, it is worth mentioning that the fabrication of such a device has seldom been reported due to the inhomogeneous and anisotropic properties of the material parameters. Thus, research on how to remove the inhomogeneous properties is highly imperative.

Recently, based on the linear coordinate transformation method, 2D and three-dimensional (3D) homogeneous electromagnetic transparent device with diamond shape have been proposed.[33,34] Though each block of this diamond shaped transparent device consists of homogeneous parameters, the permeability tensors are still anisotropic, which makes the device difficult to fabricate. To further remove the inhomogeneous and anisotropic material parameters, a 2D simplified cylindrical electromagnetic transparent device[35] was developed in our previous work, where only the axial material parameters are represented as a function of radius. It should be noted that although the radial and tangential material parameters of the device are constants, in a Cartesian coordinate system the corresponding components of the material parameters are wholly anisotropic, and thus realization of this device is still a challenge. In Ref. [36], an inverse design method was used to realize 2D circular transparent devices, which enables us to obtain the material parameters of transparent devices without knowing the specific transformation function. However, it is worth mentioning that all the reported proposals are specifically for the particular symmetric geometries, which restricts their potential applications where an arbitrarily shaped geometry is required. Moreover, the existence of anisotropic material parameters is another shortage that hinders the practical realization of these devices. Therefore, it is essential to develop homogeneous transparent device with arbitrarily shaped geometries and isotropic material parameters.

Inspired by the works of Han and Wu,[37] in this paper we propose and design an n-sided arbitrarily shaped transparent device for both regular and irregular structures based on linear transformation method. The general expressions of the

*Project supported by the National Natural Science Foundation of China (Grant Nos. 61461052 and 11564044) and the Key Program of the Natural Science Foundation of Yunnan Province, China (Grant Nos. 2013FA006 and 2015FA015).

†Corresponding author. E-mail: huangming@ynu.edu.cn
‡Corresponding author. E-mail: yangjingjing@ynu.edu.cn

© 2018 Chinese Physical Society and IOP Publishing Ltd

material parameters for transparent devices are derived, and the correctness is validated by numerical simulation. Furthermore, a multilayered structure based on effective medium theory[38] is utilized to further remove the anisotropic material properties of the transparent device for both regularly and irregularly shaped structures. Full wave simulations by the finite element method are conducted to verify the performance of the designed transparent device. With this design, all of the layered material parameters are isotropic, homogeneous and non-negative, which dramatically reduces the fabrication difficulty of practical implementation. The feasibility of designing a transparent device by using natural isotropic materials instead of metamaterials would greatly reduce the difficulty of fabrication and promote the device a step further towards the practical use.

2. Theoretical analysis

Figure 1 illustrates the design concept of a transparent device. Figures 1(a) and 1(b) indicate the original space and the physical space, respectively. The key points of designing a transparent device are to transform a large region with boundaries between $c < r < a$ into a compressed region with boundaries between $b < r < a$, and to expand a small region with boundaries between $d < r < c$ into a bigger one whose boundaries are between $d < r < b$, while keeping the outer and inner boundaries of the devices unchanged during the whole transformation.

To obtain the homogeneous material properties, we use a linear transformation method that contains six unknown parameters, thus needing six equations in total to calculate them. Therefore, by dividing the original space into several triangles and transforming them into the other ones in physical space in a 2D circumstance, we can easily meet the need and assure a unique solution. Taking the i-th region $a_i d_i d_{i+1} a_{i+1}$ as an example, to derive the constitutive parameters, we first divide them into two regions (i.e., compressive region and expanded region) in the original space. We then further divide each of them into two triangles and use the corresponding transformation functions to derive the material parameters. Thus, two kinds of transformations are needed for the compressive regions and the expanded regions.

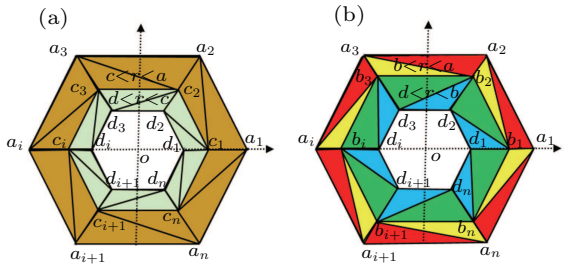


Fig. 1. (color online) Schematic diagrams of the coordinate transformation of the homogeneous transparent device, showing (a) original space and (b) physical space.

2.1. Material parameters

A concrete schematic diagram to illustrate the transformation procedure is shown in Fig. 2, in which Figs. 2(a)–2(c) and Figs. 2(d) and 2(f) indicate the compressive and expanded mappings, respectively.

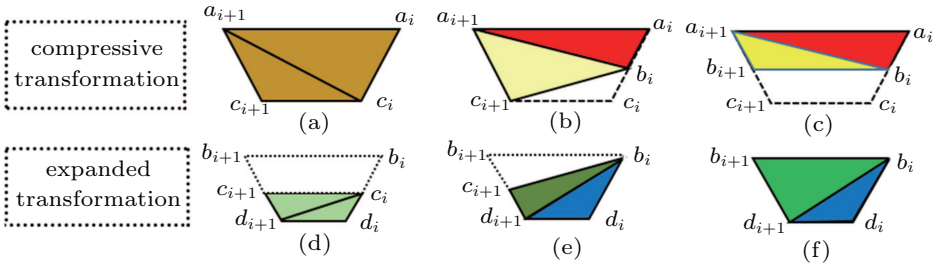


Fig. 2. (color online) Schematic diagrams of (a)–(c) the compressive transformation and (d)–(f) the expanded transformation.

First, we demonstrate how to derive the constitutive parameters of the compressive regions. According to the transformation method, the constitutive parameters of the compressive regions can be obtained by transforming $\Delta a_i a_{i+1} c_i$ and $\Delta c_i a_{i+1} c_{i+1}$ in the original space into $\Delta a_i a_{i+1} b_i$ and $\Delta b_i a_{i+1} b_{i+1}$ in the physical space, respectively, as shown in Figs. 2(a)–2(c). However, it takes two steps to achieve this goal. Above all, $\Delta a_i a_{i+1} c_i$ is transformed into $\Delta a_i a_{i+1} b_i$, and $\Delta c_i a_{i+1} c_{i+1}$ is transformed into a transitional one as $\Delta b_i a_{i+1} c_{i+1}$ as shown in Figs. 2(a) and 2(b). Then, the transitional region $\Delta b_i a_{i+1} c_{i+1}$ is further transformed into $\Delta b_i a_{i+1} b_{i+1}$ while keeping $\Delta a_i a_{i+1} b_i$ unchanged. Finally, the constitutive parameters of all regions are obtained with the value of i changing from 1 to n. It should be noted that when $i = 1$, a_{i-1}, b_{i-1}, and c_{i-1} are denoted as a_n, b_n, and c_n, respectively. Similarly, when $i = n$, a_{i+1}, b_{i+1}, and c_{i+1} are denoted as a_1, b_1, and c_1, respectively, as shown in Fig. 1.

Firstly, we derive the material parameter of $\Delta a_i a_{i+1} b_i$, which is transformed from $\Delta a_i a_{i+1} c_i$. The corresponding transformation equations can be expressed as follows:

$$\begin{aligned} x' &= m_1 x + m_2 y + m_3, \\ y' &= n_1 x + n_2 y + n_3, \\ z' &= z, \end{aligned} \tag{1}$$

where

$$\begin{bmatrix} m_1 & n_1 \\ m_2 & n_2 \\ m_3 & n_3 \end{bmatrix} = A^{-1} \begin{bmatrix} x_{a_i} & y_{a_i} \\ x_{a_{i+1}} & y_{a_{i+1}} \\ x_{b_i} & y_{a_i} \end{bmatrix}, \quad A = \begin{bmatrix} x_{a_i} & y_{a_i} & 1 \\ x_{a_{i+1}} & y_{a_{i+1}} & 1 \\ x_{c_i} & y_{c_i} & 1 \end{bmatrix}.$$

The Jacobian matrices of Eq. (1) and its corresponding determinant is given by

$$\Lambda = \begin{bmatrix} m_1 & m_2 & 0 \\ n_1 & n_2 & 0 \\ 0 & 0 & 1 \end{bmatrix}, \quad \det\Lambda = m_1 n_2 - m_2 n_1. \tag{2}$$

According to the transformation optics theory, the permeability tensor and permittivity of $\Delta a_i a_{i+1} b_i$ should be

$$\begin{aligned} \mu'_{\text{comp_outer}} &= \mu \begin{bmatrix} (m_1^2+m_2^2)/(m_1n_2-m_2n_1) & (m_1n_1+m_2n_2)/(m_1n_2-m_2n_1) \\ (m_1n_1+m_2n_2)/(m_1n_2-m_2n_1) & (n_1^2+n_2^2)/(m_1n_2-m_2n_1) \end{bmatrix}, \\ \varepsilon'_{\text{comp_outer}} &= \varepsilon/(m_1n_2-m_2n_1), \end{aligned} \tag{3}$$

where μ and ε are the permeability and permittivity of the original space, and comp_outer indicates the outer triangle of the compressive region.

Next, we continue to derive the material parameter of $\Delta b_i a_{i+1} b_{i+1}$, which is transformed from a transitional region $\Delta b_i a_{i+1} c_{i+1}$. Noting that the transitional region $\Delta b_i a_{i+1} c_{i+1}$ is further transformed from $\Delta c_i a_{i+1} c_{i+1}$, two steps should be taken to derive the material parameters.

First, $\Delta c_i a_{i+1} c_{i+1}$ is transformed into $\Delta b_i a_{i+1} c_{i+1}$, and the transformation equation can be expressed as

$$\begin{aligned} x'' &= p_1 x + p_2 y + p_3, \\ y'' &= q_1 x + q_2 y + q_3, \\ z'' &= z, \end{aligned} \tag{4}$$

where

$$\begin{bmatrix} p_1 & q_1 \\ p_2 & q_2 \\ p_3 & q_3 \end{bmatrix} = C^{-1} \begin{bmatrix} x_{b_i} & y_{b_i} \\ x_{a_{i+1}} & y_{a_{i+1}} \\ x_{c_{i+1}} & y_{c_{i+1}} \end{bmatrix}, \quad C = \begin{bmatrix} x_{c_i} & y_{c_i} & 1 \\ x_{a_{i+1}} & y_{a_{i+1}} & 1 \\ x_{c_{i+1}} & y_{c_{i+1}} & 1 \end{bmatrix}.$$

Second, the transitional region $\Delta b_i a_{i+1} c_{i+1}$ is further transformed into $\Delta b_i a_{i+1} b_{i+1}$, and the transformation equations can be expressed as

$$\begin{aligned} x' &= r_1 x'' + r_2 y'' + r_3, \\ y' &= s_1 x'' + s_2 y'' + s_3, \\ z' &= z''. \end{aligned} \tag{5}$$

where

$$\begin{bmatrix} r_1 & s_1 \\ r_2 & s_2 \\ r_3 & s_3 \end{bmatrix} = D^{-1} \begin{bmatrix} x_{b_i} & y_{b_i} \\ x_{a_{i+1}} & y_{a_{i+1}} \\ x_{b_{i+1}} & y_{b_{i+1}} \end{bmatrix}, \quad D = \begin{bmatrix} x_{b_i} & y_{b_i} & 1 \\ x_{a_{i+1}} & y_{a_{i+1}} & 1 \\ x_{c_{i+1}} & x_{c_{i+1}} & 1 \end{bmatrix}.$$

The Jacobian matrices of Eqs. (4) and (5) can be expressed as

$$\Lambda_1 = \begin{bmatrix} p_1 & p_2 & 0 \\ q_1 & q_2 & 0 \\ 0 & 0 & 1 \end{bmatrix}, \quad \Lambda_2 = \begin{bmatrix} r_1 & r_2 & 0 \\ s_1 & s_2 & 0 \\ 0 & 0 & 1 \end{bmatrix}. \tag{6}$$

The constitutive permittivity and permeability tensor of the triangle $\Delta b_i a_{i+1} b_{i+1}$ can then be obtained by

$$\begin{aligned} \varepsilon' &= (\Lambda_2\Lambda_1)\varepsilon(\Lambda_2\Lambda_1)^{\mathrm{T}}/\det(\Lambda_2\Lambda_1), \\ \mu' &= (\Lambda_2\Lambda_1)\mu(\Lambda_2\Lambda_1)^{\mathrm{T}}/\det(\Lambda_2\Lambda_1). \end{aligned} \tag{7}$$

Substitute Λ_1 and Λ_2 into Eqs. (8), the permeability tensor and permittivity of $\Delta b_i a_{i+1} b_{i+1}$ should be

$$\begin{aligned} \mu'_{\text{comp_inner}} &= \mu \begin{bmatrix} (M_1^2+M_2^2)/(M_1N_2-M_2N_1) & (M_1N_1+M_2N_2)/(M_1N_2-M_2N_1) \\ (M_1N_1+M_2N_2)/(M_1N_2-M_2N_1) & (N_1^2+N_2^2)/(M_1N_2-M_2N_1) \end{bmatrix}, \\ \varepsilon'_{\text{comp_inner}} &= \varepsilon/(M_1N_2-M_2N_1), \end{aligned} \tag{8}$$

where $M_1 = r_1p_1 + r_2q_1$, $M_2 = r_1p_2 + r_2q_2$, $N_1 = s_1p_1 + s_2q_1$, $N_2 = s_1p_2 + s_2q_2$, and comp_inner denotes the inner triangle of the compressive region.

We then derive the constitutive parameters of the expanded region. Figures 2(d)–2(f) demonstrate the schematic diagram of the detailed procedures, from which two small regions $\Delta d_i c_i d_{i+1}$ and $\Delta c_i c_{i+1} d_{i+1}$ in the original space are transformed into two big regions $\Delta d_i b_i d_{i+1}$ and $\Delta b_i b_{i+1} d_{i+1}$ in the physical space, respectively.

When we derive the constitutive parameters of the $\Delta b_i b_{i+1} d_{i+1}$, it has to be noted that there are two steps; i.e, $\Delta c_i c_{i+1} d_{i+1}$ in the original space is first transformed into transitional area $\Delta b_i c_{i+1} d_{i+1}$, and then further transformed into $\Delta b_i b_{i+1} d_{i+1}$. During the implementation of the procedure, the $\Delta c_i c_{i+1} d_{i+1}$ is transformed into the transitional $\Delta b_i c_{i+1} d_{i+1}$, and the corresponding transformation equations can be expressed as

$$\begin{aligned} x'' &= e_1 x + e_2 y + e_3, \\ y'' &= f_1 x + f_2 y + f_3, \\ z'' &= z, \end{aligned} \tag{9}$$

where

$$\begin{bmatrix} e_1 & f_1 \\ e_2 & f_2 \\ e_3 & f_3 \end{bmatrix} = E^{-1} \begin{bmatrix} x_{b_i} & y_{b_i} \\ x_{c_{i+1}} & y_{c_{i+1}} \\ x_{d_{i+1}} & y_{d_{i+1}} \end{bmatrix}, \quad E = \begin{bmatrix} x_{c_i} & y_{c_i} & 1 \\ x_{c_{i+1}} & y_{c_{i+1}} & 1 \\ x_{d_{i+1}} & y_{d_{i+1}} & 1 \end{bmatrix}.$$

Then, the transitional region $\Delta b_i c_{i+1} d_{i+1}$ is further transformed into a triangle region $\Delta b_i b_{i+1} d_{i+1}$, and the transformation equations can be expressed as

$$\begin{aligned} x' &= u_1 x'' + u_2 y'' + u_3, \\ y' &= v_1 x'' + v_2 y'' + v_3, \\ z' &= z'', \end{aligned} \tag{10}$$

where

$$\begin{bmatrix} u_1 & v_1 \\ u_2 & v_2 \\ u_3 & v_3 \end{bmatrix} = F^{-1} \begin{bmatrix} x_{b_i} & y_{b_i} \\ x_{b_{i+1}} & y_{b_{i+1}} \\ x_{d_{i+1}} & y_{d_{i+1}} \end{bmatrix}, \quad F = \begin{bmatrix} x_{b_i} & y_{b_i} & 1 \\ x_{c_{i+1}} & y_{c_{i+1}} & 1 \\ x_{d_{i+1}} & y_{d_{i+1}} & 1 \end{bmatrix}.$$

The Jacobian matrix of Eqs. (10) and (11) can be expressed as

$$\Lambda_3 = \begin{bmatrix} e_1 & e_2 & 0 \\ f_1 & f_2 & 0 \\ 0 & 0 & 1 \end{bmatrix}, \quad \Lambda_4 = \begin{bmatrix} u_1 & u_2 & 0 \\ v_1 & v_2 & 0 \\ 0 & 0 & 1 \end{bmatrix}. \tag{11}$$

The constitutive permittivity and permeability of the $\Delta b_i b_{i+1} d_{i+1}$ should be

$$\begin{aligned} \mu'_{\text{exp_outer}} &= \mu \begin{bmatrix} (S_1^2+S_2^2)/(S_1T_2-S_2T_1) & (S_1T_1+S_2T_2)/(S_1T_2-S_2T_1) \\ (S_1T_1+S_2T_2)/(S_1T_2-S_2T_1) & (T_1^2+T_2^2)/(S_1T_2-S_2T_1) \end{bmatrix}, \\ \varepsilon'_{\text{exp_outer}} &= \varepsilon/(S_1T_2-S_2T_1), \end{aligned} \tag{12}$$

where $S_1 = u_1e_1 + u_2f_1$, $S_2 = u_1e_2 + u_2f_2$, $T_1 = v_1e_1 + v_2f_1$, $T_2 = v_1e_2 + v_2f_2$, and exp_outer represents the outer triangle of the expanded region.

Finally, we derive the parameters of $\Delta d_i b_i d_{i+1}$ that is transformed from $\Delta d_i c_i d_{i+1}$, and the corresponding transformation equations are given by

$$\begin{aligned} x'' &= g_1 x + g_2 y + g_3, \\ y'' &= h_1 x + h_2 y + h_3, \\ z'' &= z, \end{aligned} \tag{13}$$

where

$$\begin{bmatrix} g_1 & h_1 \\ g_2 & h_2 \\ g_3 & h_3 \end{bmatrix} = G^{-1} \begin{bmatrix} x_{d_i} & y_{d_i} \\ x_{b_i} & y_{b_i} \\ x_{d_{i+1}} & y_{d_{i+1}} \end{bmatrix}, \quad G = \begin{bmatrix} x_{d_i} & y_{d_i} & 1 \\ x_{c_i} & y_{c_i} & 1 \\ x_{d_{i+1}} & y_{d_{i+1}} & 1 \end{bmatrix}.$$

The Jacobian matrix of Eq. (13) and its corresponding determinants are obtained by

$$\Lambda = \begin{bmatrix} g_1 & g_2 & 0 \\ h_1 & h_2 & 0 \\ 0 & 0 & 1 \end{bmatrix}, \quad \det\Lambda = g_1h_2 - g_2h_1. \tag{14}$$

The constitutive parameters of $\Delta d_i b_i d_{i+1}$ can then be derived as follows:

$$\begin{aligned} \mu'_{\text{exp_inner}} &= \mu \begin{bmatrix} (g_1^2+g_2^2)/(g_1h_2-g_2h_1) & (g_1h_1+g_2h_2)/(g_1h_2-g_2h_1) \\ (g_1h_1+g_2h_2)/(g_1h_2-g_2h_1) & (h_1^2+h_2^2)/(g_1h_2-g_2h_1) \end{bmatrix}, \\ \varepsilon'_{\text{exp_inner}} &= \varepsilon/(g_1h_2-g_2h_1), \end{aligned} \tag{15}$$

where exp_inner denotes the inner triangle of the expanded region.

Obviously, the parameters of the concentrator region are homogeneous because they are merely dependent on the vertex coordinates of the polygons.

In the regular n-sided polygonal transparent devices, the N-sided polygons A, B, and C share the same center at origin (0, 0) as shown in Fig. 1(a). Thus, the general expression of the i-th vertex of polygons A, B, and C can be defined as

$$\begin{aligned} x_{ai} &= a\cos[(i-1)2\pi/N], \quad y_{ai} = a\sin[(i-1)2\pi/N], \\ x_{bi} &= b\cos[(i-1)2\pi/N], \quad y_{bi} = b\sin[(i-1)2\pi/N], \\ x_{ci} &= c\cos[(i-1)2\pi/N], \quad y_{ci} = c\sin[(i-1)2\pi/N], \end{aligned} \tag{16}$$

where $1 \le i \le N$, and a, b, c are the circumradius of the i-th vertex of polygons A, B, and C, respectively.

However, in regard to the arbitrarily shaped asymmetric transparent device, the coordinates of each vertex of the polygons should be taken to calculate the constitutive parameters. Here, we focus on designing an arbitrarily shaped transparent device with conformal boundaries, and set the ratios of the quasi-radius (the corresponding distance from origin vertex to polygonal vertex) as $b_i = 3a_i/4$, $c_i = 3a_i/5$, and $d_i = a_i/2$. It should be noted that the aforementioned material equations still hold true when the boundaries of the polygons A, B, C, and D are non-conformal.

2.2. Layered realization of electromagnetic transparent device

Apparently, the constitutive parameters of the transparent device that we developed here are homogeneous but anisotropic, thus it is a challenge to fabricate the device.

However, the layered structure based on effective medium theory[38] provides an approach to realizing such a homogeneous and anisotropic device, where two alternate layers with homogeneous and isotropic permittivity and permeability can be utilized to achieve the equivalent of a single homogeneous anisotropic medium, if the number of the layers is large enough and the thickness of each layer is much less than the incident wavelength.[39] A schematic diagram of the layered transparent device is shown in Fig. 3. Under the transverse electric (TE) wave mode, the effective material parameters of a 2D layered device for each triangular region take the following form:

$$\mu_i^{\mathrm{A,B}} = \mu_i^u \pm \sqrt{\mu_i^u(\mu_i^u - \mu_i^v)}, \quad \varepsilon_i^{\mathrm{A,B}} = \varepsilon_{zz}, \tag{17}$$

$$\theta_i = \tan^{-1}[2\mu_{xy}^i/(\mu_{xx}^i - \mu_{yy}^i)]/2, \tag{18}$$

where $\mu_i^{u,v} = [\mu_{xx}^i + \mu_{yy}^i \pm \sqrt{(\mu_{xx}^i - \mu_{yy}^i)^2 + 4(\mu_{xy}^i)^2}]/2$.

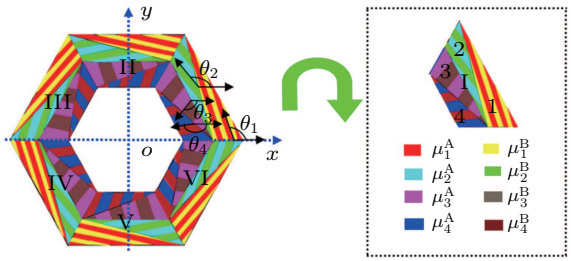


Fig. 3. (color online) A schematic diagram of the design of 2D layered electromagnetic transparent device.

Figure 3 schematically shows the 2D layered transparent device under TE wave polarization, in which: Roman numerals I–VI denote the six parts of the device; areas 1 and 2 indicate the outer and inner layer of the compressive region; and areas 3 and 4 indicate the outer and inner layer of the expanded region.

Using Eqs. (17) and (18), it is easy to obtain the material parameters and the unique rotation angle between the layer and horizontal direction of the layered structure device.

3. Results and discussion

In this section, both the regularly and irregularly shaped transparent devices are designed using the proposed approach. Full-wave simulations are carried out by using the commercial finite element solver COMSOL Multiphysics to obtain the designed material parameters and show the performance and scattering properties of the electromagnetic transparent devices developed in this work.

3.1. Regular shaped transparent device and its layered realization

First of all, as an example, a six-sided regular shaped polygonal transparent device with circumradius of $a = 8$ cm, $b = 6$ cm, $c = 5$ cm, and $d = 4$ cm for polygons A, B, C, and D is chosen. In the simulation, the whole computational domain is surrounded by a perfectly matched layer that absorbs waves propagating outward from the bounded domain. Both the TE plane wave and cylindrical wave with a working frequency of 8 GHz are utilized to demonstrate the performance of the device.

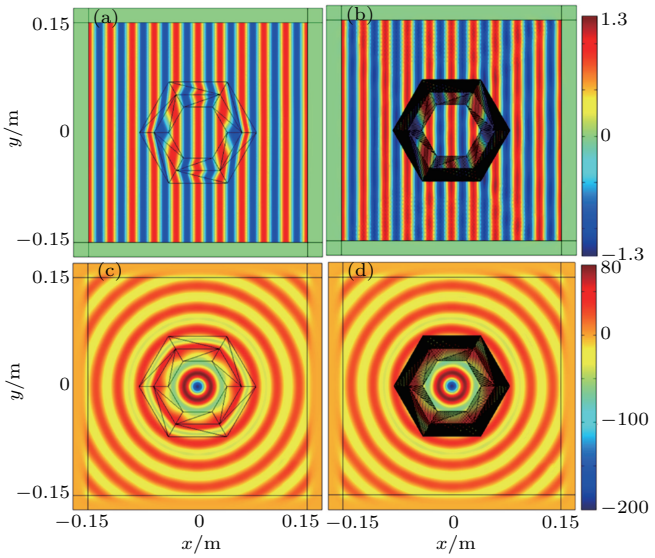


Fig. 4. (color online) Electric field distribution in the vicinity of ((a), (c)) ideal transparent and ((b), (d)) layered transparent device under irradiation of ((a), (b)) TE plane wave and ((c), (d)) cylindrical wave. The number of the divided layer is chosen to be $N = 20$.

Figure 4 illustrates the electric field distributions in the vicinity of both the ideal transparent device and its correspondent layered device under the irradiation of TE plane wave and cylindrical wave. In Fig. 4(a), the TE plane wave with the electric field polarized along the z direction is irradiated on an ideal transparent device from left to right. In Fig. 4(b), the TE plane wave identical with that in Fig. 4(a) is irradiated on a layered transparent device with 20 layers for both of isotropic dielectric materials A and B in each compressive and expanded region. Figures 4(c) and 4(d) illustrate the electric field distribution of the ideal transparent device and the layered one under cylindrical wave irradiation, where a current source of 0.01 A/m is located at (0, 0). From Figs. 4(a) and 4(b), it can be seen that although the waves are distorted in the transformation space, they return to the initial propagation direction and wave-fronts when passing through the 2D transparent device. Moreover, the layered transparent device with 20 layers behaves almost as an ideal one. From Figs. 4(c) and 4(d), it is clear that the wave-front of the cylindrical wave can be perfectly recovered when the line source is enclosed inside the transparent device for ideal and layered device. In other words, the transparent device does not affect the propagation of the cylindrical wave, which indicates that it could be used as a radome structure to protect antennas.

Figure 5 shows the scattering patterns of the perfect electric conductor (PEC) cylinder and a horn antenna covered by the transparent device. The TE wave is incident from an oblique direction with an angle of $\pi/4$. The scattering pattern of the bare PEC cylinder exposed to the free space is shown in Fig. 5(a). In Figs. 5(b) and 5(c), the PEC cylinder is covered by the ideal and layered transparent device, respectively, and also shown is the scattering pattern of the whole structure. From Figs. 5(a)–5(c), it can be seen that the field scattering of PEC cylinder with and without transparent device are almost identical with each other, revealing the capability of the device in antenna or radar protection. To further investigate the performance of the transparent device, the electric field distribution of a horn antenna without and with transparent device are investigated as shown in Figs. 5(d)–5(f). In comparison with the wave propagation of the antenna, it can be clearly seen that their field distributions are identical with each other, which also reveals the effectiveness of the transparent device in antenna protection.

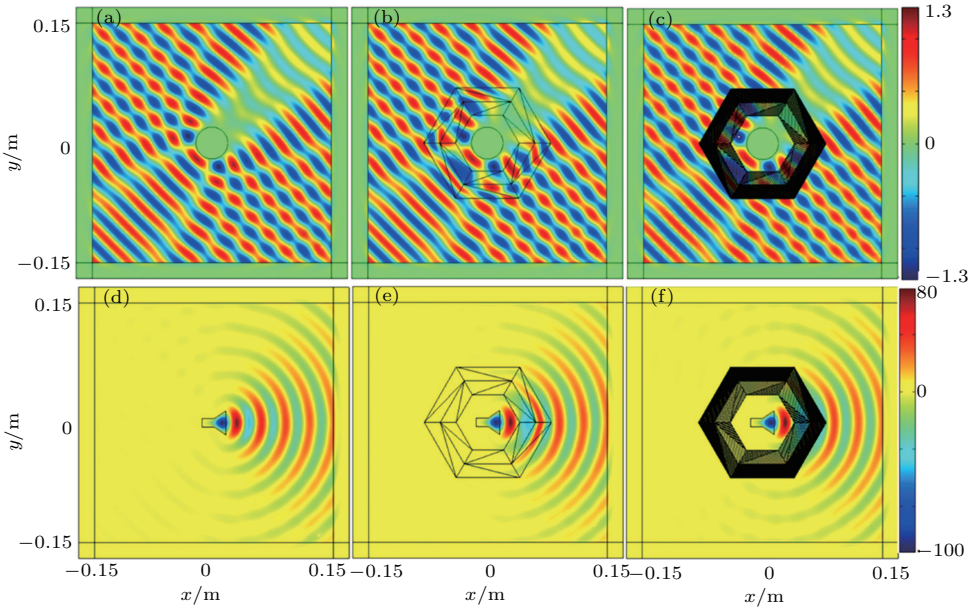


Fig. 5. (color online) (a)–(c) Scattering pattern of perfect electric conductor (PEC) cylinder and (d)–(e) wave propagation of a horn antenna covered by the transparent device. ((a), (d)) free space, ((b), (e)) horn antenna covered by ideal transparent device, ((c), (f)) horn antenna covered by layered transparent device.

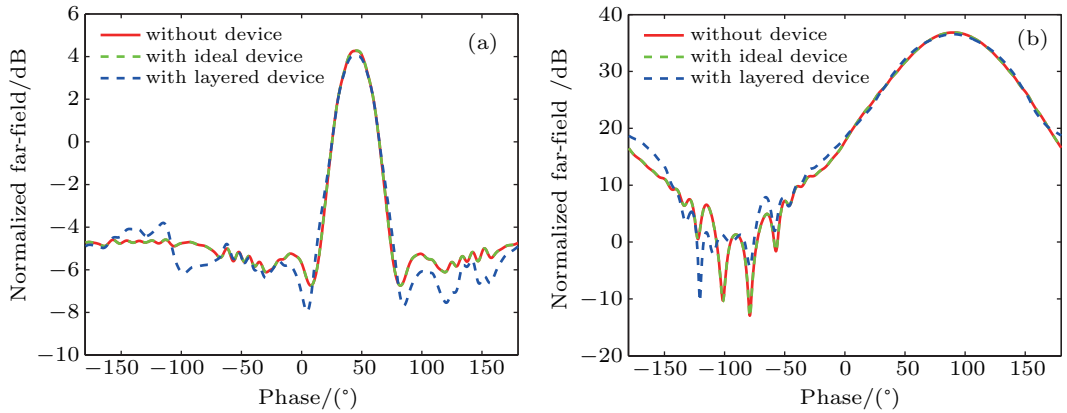


Fig. 6. (color online) Normalized far-field intensity distributions of (a) PEC cylinder and (b) horn antenna with and without transparent device.

To quantitatively evaluate the performance of the transparent device, the normalized far-field distributions of the PEC cylinder and the horn antenna with and without the transparent device are investigated, and the results are shown in Figs. 6(a) and 6(b), respectively. The red-dashed line, green-dashed line, and blue line in Fig. 6(a) denote the normalized far field of the PEC cylinder without the transparent device, a PEC cylinder covered by the ideal transparent device, and the PEC cylinder covered by layered transparent device, respectively. It is obvious that the scattering patterns of the PEC without and with the ideal transparent device are perfectly consistent, which verifies that the device acts as an ideal transparent device and has no influence on the scattering of the PEC cylinder. Moreover, it seems that small perturbation of the scattering field

appears in the layered transparent device. However, it is almost negligible. Similarly, the normalized far electric fields of a horn antenna without and with the ideal and layered transparent devices are investigated as shown in Fig. 6(b), where the red-dashed line, green line and blue-dashed line indicate the horn antenna in free space, the horn antenna enclosed by the ideal transparent device, and the horn antenna covered by layered structure transparent device, respectively. Again, the three cases obtain the almost identical field profile, serving as an evidence of the perfect transparent properties of the device. Thus, it is concluded that the transparent device can be used as a radome structure to protect an antenna from being affected by adverse weather conditions, thus guaranteeing the stability and durability of the antenna during its life-time.

3.2. Irregular shaped transparent device and its layered realization

In this section, we utilize the material parameters' equations derived above to design the irregular arbitrarily-shaped concentrators and realize them with the layered structures. The vertices of the outer polygon A for the transparent device are chosen to be $a_1 = (0.1\ \text{m},\ 0.01\ \text{m})$, $a_2 = (0.05\ \text{m},\ 0.08\ \text{m})$, $a_3 = (-0.04\ \text{m},\ 0.08\ \text{m})$, $a_4 = (-0.09\ \text{m},\ -0.03\ \text{m})$, $a_5 = (0,\ -0.07\ \text{m})$, and $a_6 = (0.09\ \text{m},\ -0.05\ \text{m})$. The vertex coordinates of the polygons B, C, and D can be easily calculated from expressions $b_i = 3a_i/4$, $c_i = 3a_i/5$, and $d_i = a_i/2$.

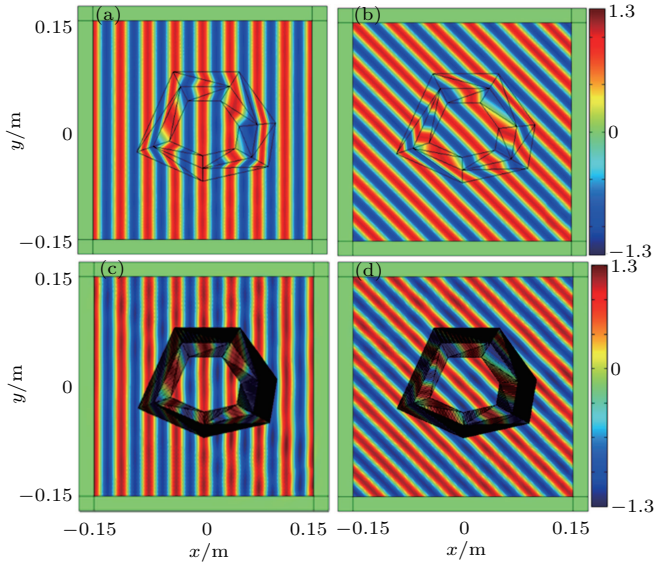


Fig. 7. (color online) Electric field distribution in the vicinity of ((a), (b)) arbitrary shaped ideal transparent device and ((c), (d)) layered transparent device. (a) and (c) TE plane wave incident from horizontal direction. (b) and (d) TE plane wave incident from an oblique direction with angle $\pi/4$.

Figure 7 demonstrates the electric field distribution in the vicinity of the irregular shaped ideal transparent device and the layered transparent device. In Figs. 7(a) and 7(c), the TE plane wave is incident from the horizontal direction. Meanwhile, in Figs. 7(b) and 7(d), it is incident from an oblique direction with an angle of $\pi/4$. The number of the divided layers is chosen to be $N = 20$ for all the isotropic media utilized in the layered transparent device. The results show that the prominent performance of the device is irrespective of the direction of incidence wave. This means that the device is capable of being used as a radome structure to protect antennas.

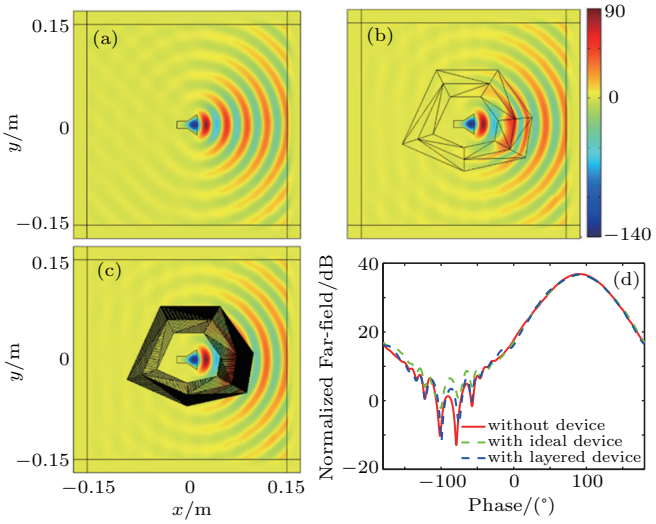


Fig. 8. (color online) ((a)–(c)) Near field distribution and (d) normalized far field distribution in the vicinity of the horn antenna (a) without and ((b), (c)) with the transparent device. (b) Horn antenna covered by ideal transparent device. (c) Horn antenna covered by a layered transparent device.

To further examine whether the proposed arbitrarily shaped transparent device can be used to protect the antenna in practical applications, the electric field distribution in the vicinity of a horn antenna covered separately by the ideal and the layered transparent device are investigated, as shown in Figs. 8(b) and 8(c). The number of the divided layers in Fig. 8(c) is chosen to be $N = 20$ and the line source with a current of 0.01 A/m is located at (0, 0), acting as an excitation source. By comparison, the electric field distribution of a horn antenna without the transparent device is also investigated as shown in Fig. 8(a). It is obvious that both cases of the horn antenna covered separately by the ideal transparent device and layered structure yield the electric field distribution almost identical with that generated by the bare antenna without the device, which confirms the effectiveness of the device acting as a protective equipment. The corresponding normalized far fields of the three cases above are illustrated in Fig. 8(d), where the red line, blue-dashed line and green-dashed line indicate the horn antenna without the transparent device, with the ideal transparent and with the layered structure device, respectively. The results show that the normalized far field distribution of the horn antenna with and without the transparent device are almost the same.

3.3. Influence of the divided layers

In this subsection, we investigate the influence of the divided layers on the performance of the transparent device. A

6-sided regular polygonal transparent device is utilized to investigate the relationship between the transparent property and the number of layers. For convenience, a Gaussian beam with a wavelength of 0.3 m and beam width of 0.9 m is utilized in the simulation.

Figures 9(a)–9(c) show the electric field distribution of the Gaussian beam in the vicinity of the layered structure transparent devices with 10, 20, and 30 divided layers, respectively. By comparison, the electric field distribution in the vicinity of the ideal transparent device is also investigated as shown in Fig. 9(d). It can be clearly seen that when the number of the divided layers is configured as $N = 10$, the field disturbance of the device is relatively strong, making the field distribution of the layered structure device distinguishable from the ideal one, as shown in Fig. 9(a). That is to say, the transparent performance of the layered device is not perfect when the number of the layers is not large enough. However, when the number of the divided layers reaches $N = 20$, the disturbance almost disappears and the difference between the layered device and ideal device becomes negligible, as shown in Fig. 9(b). By further increasing the divided layers to $N = 30$, the performance of the layered transparent device is almost identical with that of the ideal one as shown in Fig. 9(c).

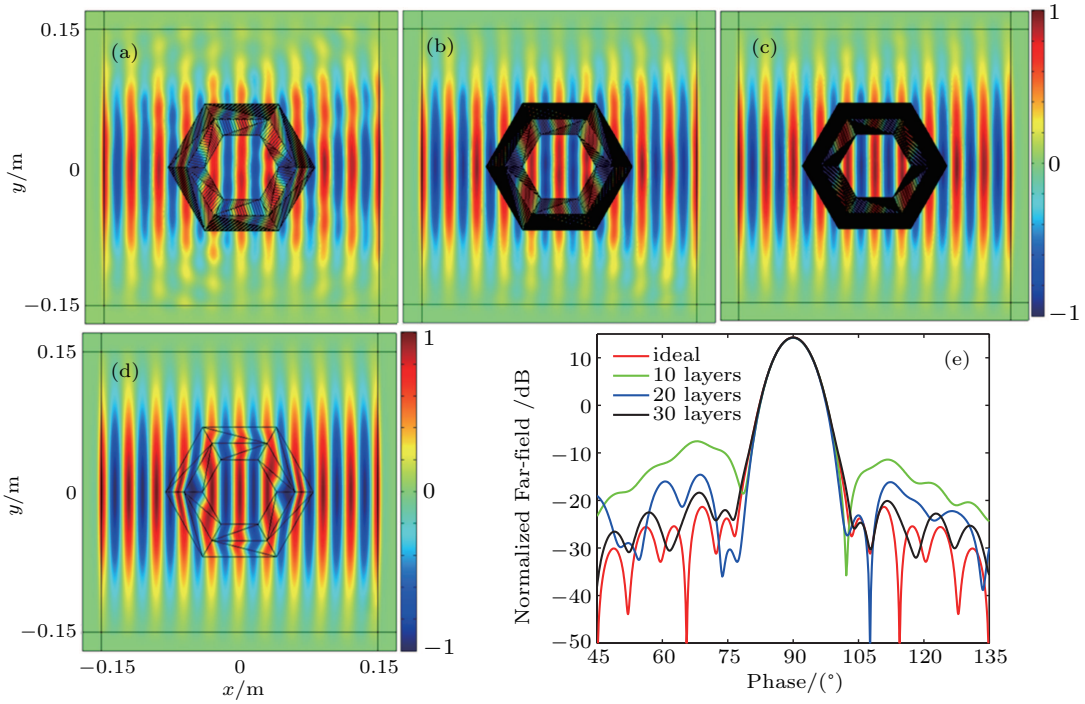


Fig. 9. (color online) (a)–(d) Near electric field distributions, and (e) normalized far field distribution of ((a)–(c)) layered transparent device and (d) ideal transparent device. The number of divided layers $N = 10$ (a), 20 (b), 30 (c).

To quantitatively evaluate the performance of the layered transparent device, the normalized far field in the right boundary of the computational region under the Gaussian beam irradiation is calculated as shown in Fig. 9(e), where the solid line, green line, blue line, and black line indicate the normalized far field of the ideal transparent, layered transparent with $N = 10$, $N = 20$, and $N = 30$, respectively. It can be clearly seen that when $N = 10$, the disturbance of the normalized field is strong, and the difference between the ideal transparent device and layered one is obvious. However, when the number of the divided layers is increased to $N = 20$, the difference between them is greatly reduced: the difference is small enough to be negligible. The difference is further reduced when the number of the divided layers reaches to $N = 30$. Theoretically speaking, the difference between the ideal and layered transparent device will totally disappear when the number of divided layers is large enough. However, with the increase of the number of layers, more computation memory and time are taken to obtain a finer mesh for the computational domain around the layered device.

4. Conclusions

In this work, based on the linear coordinate transformation optics, 2D electromagnetic transparent devices with arbitrary regularly and irregularly shaped cross section are proposed and designed. In contrast to the reported transparent devices, the proposed devices possess the material parameters that are homogeneous, anisotropic, positive and generic, which makes the design approach more flexible and applicable to practical fabrication. Furthermore, a multilayered structure is utilized to remove the anisotropic property of the device, making the whole device realizable only by using the naturally

positive isotropic materials. The numerical results show that the layered device with sufficient layers possesses the performance as nearly perfect as the ideal one and is capable of protecting antennas without sacrificing the performance. The feasibility of designing a transparent device by ordinary isotropic materials instead of metamaterials would dramatically reduce the difficulty of fabrication and improve the practicality of the device. It is believed that the scheme presented in this work could be used to design other electromagnetic devices. The method can also be extended to the 3D structures or other branches of physics, such as acoustics and thermodynamics.

References

[1] Pendry J B, Schurig D and Smith D R 2006 *Science* **312** 1780
[2] Leonhardt U 2006 *Science* **312** 1777
[3] Chen H Y, Chan C T and Sheng P 2010 *Nat. Mater.* **9** 387
[4] Liu R, Ji C, Mock J J, Chin J Y, Cui T J and Smith D R 2009 *Science* **323** 366
[5] Lai Y, Chen H, Zhang Z Q and Chan C T 2009 *Phys. Rev. Lett.* **102** 093901
[6] Valentine J, Li J, Zentgraf T, Bartal G and Zhang X 2009 *Nat. Mater.* **8** 568
[7] Han T, Tang X and Xiao F 2009 *J. Phys. D: Appl. Phys.* **42** 235403
[8] Yang J J, Huang M, Yang C F and Yu J 2011 *Eur. Phys. J. D* **61** 731
[9] Wong Z J, Wang Y, O'Brien K, Rho J, Yin X, Zhang S and Zhang X 2017 *J. Opt.* **19** 084007
[10] Zheng B, Madni H A, Hao R, Zhang X, Liu X, Li E and Chen H 2016 *Light-Sci. Appl.* **5** e16177
[11] Rajput A and Srivastava K V 2017 *Plasmonics* **12** 771
[12] Madni H A, Hussain K, Jiang W X, Liu S, Aziz A, Iqbal S and Cui T J arXiv: 1805.05403
[13] Luo X Y, Liu D Y, Liu J J and Dong J F 2014 *Chin. Phys. B* **23** 054101
[14] Liu G C, Li C, Shao J J, F and G Y 2014 *Chin. Phys. Lett.* **31** 044101
[15] Zang X F, Zhu Y M, Ji X B, Chen L, Hu Q and Zhuang S L 2017 *Sci. Rep.* **7** 40941
[16] Jiang W X, Cui T J, Yang X M, Ma H F and Cheng Q 2011 *Appl. Phys. Lett.* **98** 204101
[17] Li T H, Huang M, Yang J, Xu X and Chen M 2015 *Mod. Phys. Lett. B* **29** 1550045
[18] Zhang K, Ding X, Wo D, Meng F and Wu Q 2016 *Appl. Phys. Lett.* **108** 053508
[19] Jiang W X, Bao D and Cui T J 2016 *J. Opt.* **18** 044022
[20] Wang H, Deng Y, Zheng B, Li R, Jiang Y, Dehdashti S and Chen H 2017 *Sci. Rep.* **7** 40083
[21] Yang R, Kong X, Wang H, Su H, Lei Z, Wang J and Chen L 2016 *Sci. Rep.* **6** 20530
[22] Eskandari H, Majedi M S and Attari A R 2017 *JOSA B* **34** 1191
[23] Wu Y L, Zhuang Z, Deng L and Liu Y A 2016 *Sci. Rep.* **6** 24495
[24] Mei J S, Wu Q, Zhang K, He X J and Wang Y 2016 *Opt. Commun.* **368** 113
[25] Yu Z Z, Feng Y J, Wang Z B, Zhao J M and Jiang T C 2013 *Chin. Phys. B* **22** 034102
[26] Chen X, Cai L and Wen J H 2018 *Chin. Phys. B* **27** 057803
[27] Zhang K L, Hou Z L, Bi S and Fang H M 2017 *Chin. Phys. B* **26** 0127802
[28] Xia G, Kou W, Yang L and Du Y C 2017 *Chin. Phys. B* **26** 0104403
[29] Wang Y Y, Ding E L, Liu X Z and Gong X F 2016 *Chin. Phys. B* **25** 0124305
[30] Yu G X, Cui T J and Jiang W 2009 *J. Infrared. Millim. T. E* **30** 633
[31] Yang C F, Yang J J, Huang M, Shi J H and Peng J H 2010 *RadioEng.* **19** 136
[32] Mei Z L, Niu T M, Bai J and Cui T J 2010 *J. Appl. Phys.* **107** 124908
[33] Yang J J, Li T H, Huang M and Cheng M 2011 *Appl. Phys. A* **104** 733
[34] Li T, Huang M, Yang J, Yu J and Lan Y 2011 *J. Phys. D: Appl. Phys.* **44** 325102
[35] Li T, Huang M, Yang J J, Xie, R S and Yu J 2012 *Int. J. Rf. Microw. C E* **22** 522
[36] Li T H, Huang M, Yang J J, Yang G and Cai G H 2014 *Chin. Phys. B* **23** 054102
[37] Han T and Wu Z 2014 *Opt. Lett.* **39** 3698
[38] Wood B, Pendry, J B and Tsai D P 2006 *Phys. Rev. B* **74** 115116
[39] Li T, Huang M, Yang J, Zhu W and Zeng J 2013 *IEEE T. Magn.* **49** 5280